Mining hyperspectral data for non-destructive and rapid prediction of nitrite content in ham sausages

Yadong Zhu[1], Hongju He[1,2,3*], Shengqi Jiang[1], Hanjun Ma[1,2], Fusheng Chen[3], Baocheng Xu[4], Hong Liu[5], Mingming Zhu[1], Shengming Zhao[1], Zhuangli Kang[1]

(1. *School of Food Science, Henan Institute of Science and Technology, Xinxiang 453003, Henan, China*;
2. *Henan Institute of Science and Technology, Postdoctoral Research Base, Xinxiang 453003, Henan, China*;
3. *College of Grain, Oil, and Food, Henan University of Technology, Zhengzhou 450000, China*;
4. *College of Food and Bioengineering, Henan University of Science and Technology, Luoyang 471003, Henan, China*;
5. *Key Laboratory of the Ministry of Education of Tropical Medicine, Hainan Normal University, Haikou 570203, China*)

Abstract: Accurate and rapid determination of nitrite contents is an important step for guaranteeing sausage quality. This study attempted to mine hyperspectral data in the range of 900-1700 nm for non-destructive and rapid prediction of nitrite contents in sausages. The average spectra of 156 samples were collected to relate to the measured nitrite values by partial least squares (PLS) regression. Optimal wavelengths were respectively selected by successive projections algorithm (SPA) and regression coefficients (RC) to simplify the PLS model. The results indicated that PLS model established with 15 optimal wavelengths (900.5 nm, 907.1 nm, 908.8 nm, 912.1 nm, 915.4 nm, 920.3 nm, 922.0 nm, 941.7 nm, 979.6 nm, 1083.2 nm, 1213.2 nm, 1353.0 nm, 1460.2 nm, 1595.6 nm and 1699.9 nm) selected by SPA had better performance with r_C, r_{CV}, r_P of 0.92, 0.89, 0.89 and RMSEC, RMSECV, RMSEP of 0.41 mg/kg, 0.89 mg/kg, 0.49 mg/kg, respectively, for calibration set, cross-validation and prediction set. It was concluded that hyperspectral data could be mined by PLS & SPA for realizing the rapid evaluation of nitrite content in ham sausages.

Keywords: hyperspectral data, ham sausage, non-destructive and rapid prediction, nitrite, partial least squares (PLS)
DOI: 10.25165/j.ijabe.20211402.5407

Citation: Zhu Y D, He H J, Jiang S Q, Ma H J, Chen F S, Xu B C, et al. Mining hyperspectral data for non-destructive and rapid prediction of nitrite content in ham sausages. Int J Agric & Biol Eng, 2021; 14(2): 182–187.

1 Introduction

Meat processing is a major branch of the food industry, and the demand for meat products for the market is increasing. As one of the popular meat products, ham sausage has consumption advantages of pleasant flavor, convenient for carrying and ready-to-eat, occupying a considerable market share[1]. Ham sausage with high quality is still highly demanded by consumers. Nitrite is one of the important additives of ham sausage and is usually used to maintain color and freshness. In other words, the nitrite content will influence the quality of ham sausages[2]. Besides, nitrite plays an indispensable role in ham sausages, by providing oxidation resistance and inhibiting the growth of microorganisms such as *Clostridium botulinum*[3]. However, excessive consumption of nitrite will lead to toxic reactions in human bodies. The World Health Organization has reported that the lethal level of nitrite intaking is in the range of 8.7 to 28.3 μmol[4,5]. But in practical production, a few producers increase the amount of nitrite to enhance color, attracting attentions of consumers and improving sales, which is however harmful to humans[6]. Therefore, it is necessary to detect nitrite content and ensure the quality of ham sausages.

At present, the methods to evaluate the nitrite contents of meat products are mainly based on spectrophotometric and electrochemical detection[7], and most methods are time-consuming, tedious, laborious and environmentally unfriendly[8]. In order to meet the demand for fast and nondestructive detection of nitrite in ham sausages, novel techniques should be considered and exploited.

It is well known that spectroscopic methods are rapid, non-destructive and environmentally friendly, especially near-infrared (NIR) spectroscopy[9]. NIR region can be used for food quality detection and control because chemical components of meat products can adsorb NIR light energy and generate the related information for quality evaluation[10].

Hyperspectral imaging technology, originally used in the field of remote sensing by the National Aeronautics and Space Administration (NASA)[9], combining the one-dimensional spectral technology and two-dimensional imaging technology to obtain spectral and spatial information of samples at the same time, has been widely used in quality assessment of meat and meat products

Received date: 2019-09-20 **Accepted date:** 2020-11-28

Biographies: Yadong Zhu, Master, research interest: food nondestructive analysis and detection, Email: zhuyd1993@126.com; **Shengqi Jiang**, Master, research interest: food nondestructive analysis and detection, Email: shq_jiang@163.com; **Hanjun Ma**, PhD, Professor, research interest: meat processing and quality control, Email: xxhjma@126.com; **Fusheng Chen**, PhD, Professor, research interest: food resource development and utilization, Email: fushengc@haut.edu.cn; **Baocheng Xu**, PhD, Associate Professor, research interest: oil component control technology, Email: xbc76@163.com; **Hong Liu**, PhD, Professor, research interest: food engineering, Email: lhyd123@126.com; **Mingming Zhu**, PhD, research interest: processing and storage of agricultural products, protein purification, Email: happyzhumingming@126.com; **Shengming Zhao**, PhD, research interest: food safety and control, E-mail: zhaoshengming2008@126.com; **Zhuangli Kang**, PhD, Associate Professor, research interest: meat processing, Email: kzlnj1988@163.com.

***Corresponding author: Hongju He**, PhD, Professor, research interest: food nondestructive analysis and detection. Henan Institute of Science and Technology, Postdoctoral Research Base, Xinxiang 453003, Henan, China. Tel: +86-373-3040674, +86-13525022325, Fax: +86-373-3040674, Email: hongju_he007@ 126.com.

in recent years[11]. Compared to traditional near-infrared technology, hyperspectral imaging technology can provide spectral information in each pixel in the acquired images for research. For example, He et al.[12] evaluated the potential of NIR hyperspectral imaging to predict *Pseudomonas* spp. counts distribution in salmon fillets, resulting in a good performance with coefficients of determination (R^2_P) of 0.91 and root mean square error of prediction (RMSEP) of 0.49 $\log_{10}$ CFU/g. Sara et al.[13] investigated the performance of different models to predict TVC value in rainbow-trout fish fillets using hyperspectral imaging and revealed good results. In addition, the hyperspectral imaging technique has also been used in the physical and chemical detection of meat products. Kamruzzaman et al.[14] developed an online system using hyperspectral imaging to monitor red meat (beef, lamb, and pork) color in the range of 400-1000 nm. Other studies[15,16] also indicated the great potential of hyperspectral imaging in meat quality evaluation. However, few studies have been reported on nitrite detection in ham sausage by hyperspectral imaging technology.

Given the advantages of hyperspectral imaging, in this study, we attempted to mine hyperspectral data in the wavelength range of 900-1700 nm to determine nitrite content in ham sausages in a rapid and noncontact way, which will provide a methodological reference for further online application in the future.

2 Materials and methods

2.1 Sample preparation

One hundred and fifty-six ham sausages with the same shelf life (six months) but different manufacture dates were supplied by a local supermarket. All ham sausages were labeled and transported to Meat Processing & Quality Control Lab, Henan Institute of Science and Technology, Xinxiang, Henan, China. According to different manufacture dates, all samples were divided into three groups for further tests. Then, a sample with a thickness of 1 cm was cut from a ham sausage, resulting in a total of 156 samples from 156 ham sausages. All the samples were evenly divided into three groups (52 samples in each group), and samples in Group I, II and III expire in 4-6 months, 2-4 months, 0-2 months, respectively.

2.2 Hyperspectral data acquisition

In this study, a push broom line-scan hyperspectral imaging system (900-1700 nm) was used to acquire hyperspectral images of the ham sausage sample in reflectance mode (Figure 1). The hyperspectral images system is mainly composed of a spectrograph (Spatial resolution of 5 nm, ImSpector V10E, Spectral Imaging Ltd, Oulu, Finland), a high-performance CCD camera (DL-604 M, Andor, Ireland), illumination units (Illumination Technologies Inc, New York, USA), a lens (the focal length of 30 mm, OLE2, Schneider, German), a translation stage (IRCP0076-1COMB, Isuzu Optics Corp, Taiwan, China) and a computer installed with Spectral Image software and HSI Analyzer software (Isuzu Optics Corp, Taiwan).

On each day, five samples from each group were placed on the moving table in hyperspectral imaging equipment and scanned by the hyperspectral images system with a moving speed of 7.13 mm/ms, the penetration depth of 1 cm and the camera exposure time of 4.25 ms in the horizontal directions. As a result, 156 hyperspectral images of samples were collected. Then, the image calibration was conducted to calibrate the raw hyperspectral images into reflectance images. The white and black images were involved to eliminate the influences of the background[17]. The whole process can be explained by a formula shown as below:

$$I_C = \frac{I_R - I_B}{I_W - I_B} \tag{1}$$

where, I_C is calibrated hyperspectral images; I_R is raw hyperspectral images; I_B is black images (0% reflectance) obtained by turning off the light source and covering the camera lens with its cap; I_W is white images obtained by scanning a uniform white tile (99.9% reflectance, Isuzu Optics Corp, Taiwan).

After the completion of image calibration, the region of interest (ROI) of each sample was identified and then automatically isolated from the background by HSI Analyzer software. The spectra (486 wavelengths with 1.67 nm interval) within all pixels of the isolated ROI were averaged and extracted and a total of 156 mean spectra (corresponding to the 156 samples) were finally obtained for further analysis.

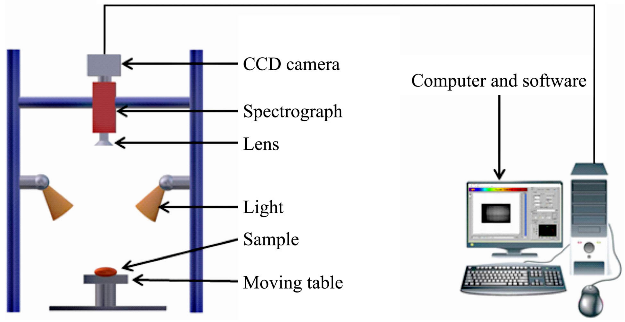

Figure 1 Schematic diagrams of main components of the hyperspectral imaging systems[25]

2.3 Nitrite content measurement

After the data extraction, the nitrite content in each sample was immediately measured by the naphthalene ethylenediamine hydrochloride method in GB5009.33-2016[18]. Firstly, the protein was precipitated and the fat was removed. Then, the nitrite and p-aminobenzene sulfonic acid was diazotized and coupled with naphthalene ethylenediamine hydrochloride to form purple-red dye under the condition of the weak acid. The content of nitrite was determined by the external standard method.

2.4 Spectral data pretreatment

It is necessary to conduct spectral data pretreatment to reduce the effect from the noise of equipment, the scattering and the surrounding environment before the spectral data analysis[19]. In this study, several pretreatment methods including moving average smoothing (MAS), Savitsky-Golay smoothing (SGS), median filter smoothing (MFS), Gaussian filter smoothing (GFS) and normalization were applied and carried out using software Unscrambler 9.7 (CAMO, Oslo, Norway)[20].

2.5 Multivariate date analysis

After spectral pretreatment, partial least square (PLS) regression was performed to establish a relationship between the mean reflectance spectral data and the measured value of nitrite[21]. PLS is one of the most robust and reliable tools for the establishment of a calibration model because it is suitable when the number of variables is more than that of samples[22]. Among the 156 samples, 104 samples were used for the establishment of the calibration model and the remaining 52 samples were used for prediction. The correlation coefficient of calibration (r_C), cross-validation (r_{CV}) and prediction (r_P), as well as the root, mean square error of calibration (RMSEC), cross-validation (RMSECV) and prediction (RMSEP) were used for the PLS model performance evaluation[23]. In general, a good PLS model has high values of r_C, r_{CV}, r_P and low values of RMSEC, RMSECV, RMSEP. Besides, the residual predictive deviation (RPD) and the absolute value between RMSEC and RMSEP were also used to assess the capability of the PLS models[24]. All the modeling operations were carried out using Unscrambler 9.7 (CAMO, Oslo, Norway).

2.6 Informative wavelengths selection and model optimization

A hyperspectral image is usually characterized by high dimensionality and collinearity among contiguous variables which requires much time to compute the hyperspectral data[26]. It is necessary to remove irrelevant wavelengths and select informative wavelengths, which will improve the model accuracy and accelerate the data analysis[27]. In this study, regression coefficients (RC) and successive projections algorithm (SPA) were respectively applied to select useful wavelengths for model optimization. In RC method, wavelengths with higher regression coefficient values (regardless of the sign) are regarded as the important wavelengths[22]. SPA is often used to solve the colinearity problems of spectral wavelengths[28]. In SPA procedure, firstly, the candidate subsets of spectra (variable X) and the measured values of nitrite content (Y) were constructed and analyzed in a matrix. Then the best constructed candidate subsets were selected according to the performance of the established model[29]. By RC and SPA methods, the optimal wavelengths were respectively selected to optimize original PLS models built with full 486 wavelengths (F-PLS). The optimized PLS models (O-PLS) were obtained and evaluated by the same parameters used in F-PLS models. The RC and SPA procedure was carried out using Unscrambler 9.7 (CAMO, Oslo, Norway) and Matlab R2010b software (The Mathworks, Inc, Natick, MA, USA), respectively.

3 Results and discussion

3.1 Reference nitrite values

The reference nitrite values of the 156 samples were calculated and shown in Table 1. In order to ensure the diversity of samples, the samples were collected according to the different manufacture dates. The content of nitrite in ham sausages changed due to the different manufacture dates. It can be seen from Table 1 that the nitrite content of the collected samples has a wide distribution range.

Table 1 Reference nitrite values (mg/kg) measured by spectrophotometric method

Sample set	Number of sample	Minimum	Maximum	Range	Mean±SD
Calibration	104	1.58	6.75	5.17	3.42±1.06
Prediction	52	1.61	6.40	4.79	3.42±1.04
Total	156	1.58	6.75	5.17	3.42±1.05

Note: SD: Standard deviation.

3.2 Spectral characteristics of ham sausage samples

It has been reported that NIR region is a very useful and informative spectral range for qualitative and quantitative analysis[30]. The typical average spectra extracted from the ham sausages in the wavelength range of 900-1700 nm are shown in Figure 2. In specific, Figure 2a shows the raw spectra, and Figures 2b, 2c, 2d, 2e, 2f show the five different pretreatment spectra, respectively. In general, the spectral curves with different nitrite content were smooth and had the same trends in the whole region. As can be seen from Figure 2, three obvious absorbance peaks are observed at around 985 nm, 1210 nm and 1450 nm in the 900-1700 nm region. Among, the intensive absorption peaks at around 980 nm and 1450 nm are related to the water content of the samples (O-H stretching second and first overtone, respectively)[31]. The absorption peak occurs at around 1210 nm originated from the fat content of samples (C-H stretching the second overtone)[32].

3.3 Nitrite prediction by F-PLS model using full wavelength

The F-PLS models were established using the full 486 wavelengths and the results were shown in Table 2. The F-PLS models based on the Raw, MAS, SGS, MFS, GFS and Normalize spectra exhibited good similar performance in predicting nitrite content in ham sausages, with r of 0.87-0.90 and RMSE of 0.41-0.53 mg/kg. In addition, the RPD values were within 2-2.5, indicating the feasibility of the six F-PLS models in predicting nitrite[33]. Also, ΔE values (|RMSEC-RMSEP|) were all close to zero, showing good robustness of the six F-PLS models[34].

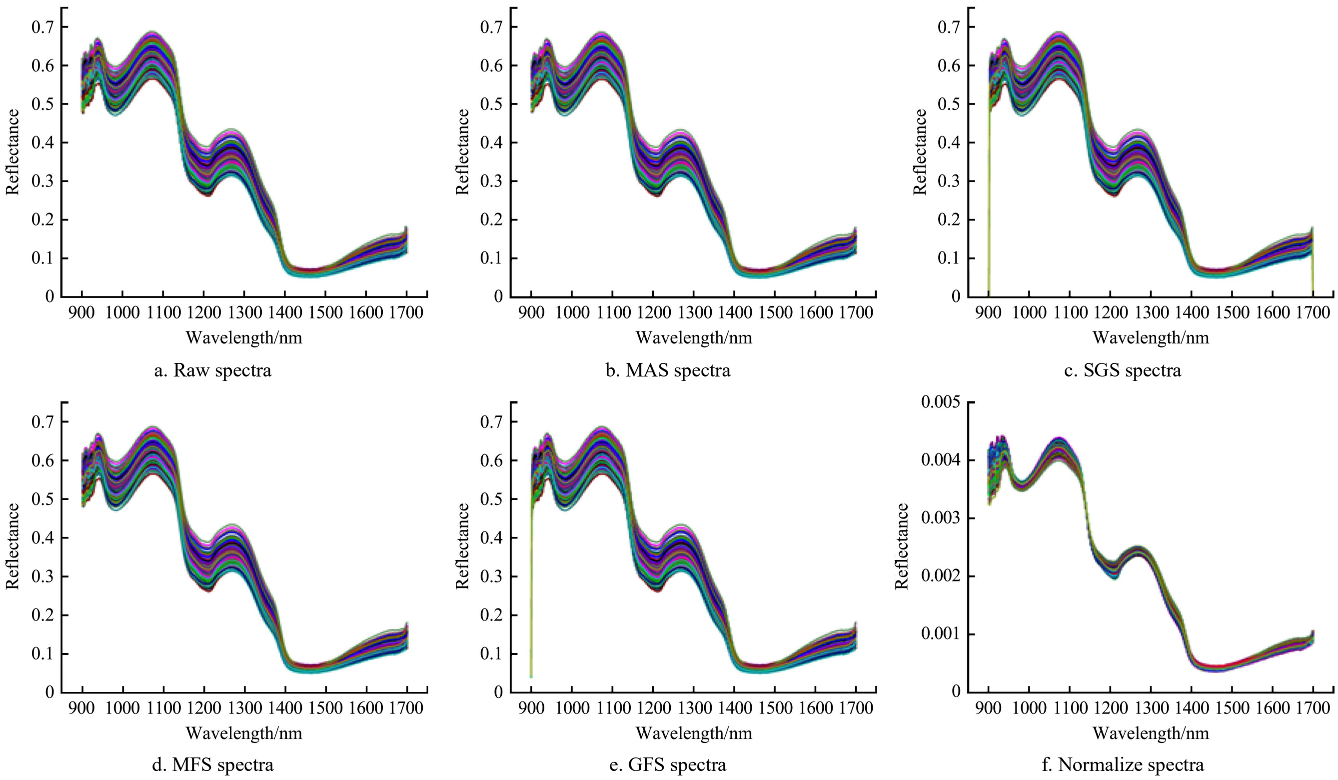

a. Raw spectra
b. MAS spectra
c. SGS spectra
d. MFS spectra
e. GFS spectra
f. Normalize spectra

Figure 2 Average spectra of ham sausage samples in the wavelength range of 900-1700 nm

Table 2 F-PLS models for predicting nitrite using full wavelengths

Spectra	LVs	Calibration		Cross-validation		Prediction			ΔE
		r_C	RMSEC/mg·kg^{-1}	r_{CV}	RMSECV/mg·kg^{-1}	r_P	RMSEP/mg·kg^{-1}	RPD	
Raw	9	0.92	0.41	0.88	0.50	0.91	0.44	2.37	0.03
MAS	9	0.91	0.44	0.87	0.52	0.90	0.46	2.30	0.02
SGS	9	0.91	0.44	0.87	0.52	0.90	0.46	2.28	0.02
MFS	9	0.91	0.44	0.87	0.53	0.91	0.44	2.37	0.00
GFS	9	0.92	0.41	0.88	0.50	0.91	0.44	2.36	0.03
Normalize	8	0.92	0.41	0.89	0.49	0.91	0.44	2.35	0.03

Note: LVs: Latent variables; RPD: residual predictive deviation; ΔE: absolute value between RMSEC and RMSEP

3.4 Selection of optimal wavelengths by RC and SPA

Although the F-PLS models with full wavelengths (486 wavelengths) had good predictive performance, the large wavelength number still requires much time to process the data[35]. To accelerate data analysis, informative wavelengths were selected from the raw spectral range by RC and SPA, and the results are shown in Figure 3 and Figure 4, respectively.

In RC method, 19 wavelengths at 902.2 nm, 908.8 nm, 912.1 nm, 913.7 nm, 918.7 nm, 933.5 nm, 936.8 nm, 991.1 nm, 1216.4 nm, 1249.3 nm, 1382.7 nm, 1384.3 nm, 1499.8 nm, 1643.6 nm, 1675.1 nm, 1693.3 nm, 1695.0 nm, 1696.6 nm and 1698.3 nm were selected as the optimal wavelengths. The wavelength number reduced 96% from the original 486 wavelengths.

In SPA method, as shown in Figure 4a, RMSE plots were acquired by operating SPA program for selecting optimal wavelengths number. The RMSE curve showed an overall fall trend as the number of optimal wavelengths increased from 1 to 15, then a gradual rise when the variable numbers increased from 15 to 20. The 15 optimal variables including 900.5 nm, 907.1 nm, 908.8 nm, 912.1 nm, 915.4 nm, 920.3 nm, 922.0 nm, 941.7 nm, 979.6 nm, 1083.2 nm, 1213.2 nm, 1353.0 nm, 1460.2 nm, 1595.6 nm and 1699.9 nm were picked and marked with a square marker, as shown in Figure 4b. The wavelength number reduced 97% from the original 486 wavelengths.

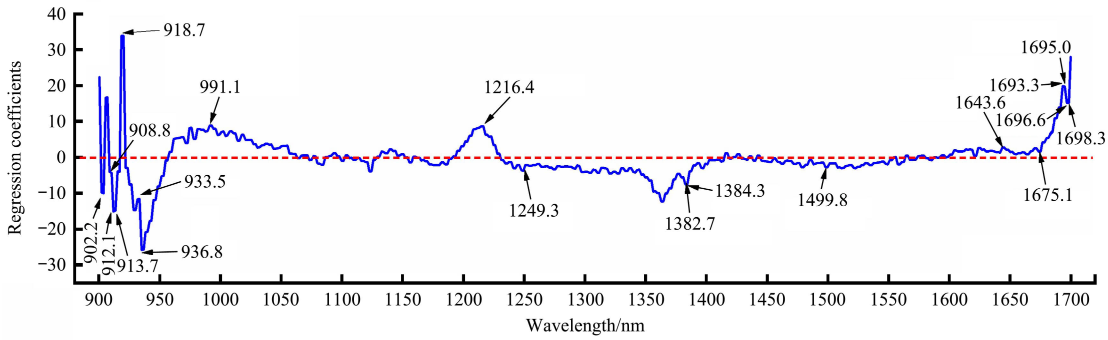

Figure 3 Selection of optimal wavelengths by RC method

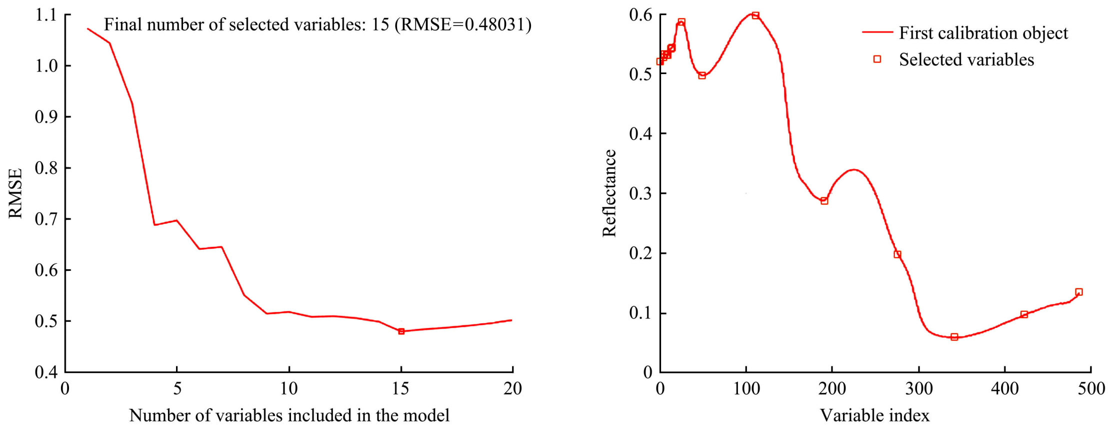

a. Number of variables included in the model

b. Optimal wavelength location

Figure 4 Selection of optimal wavelengths by SPA method

3.5 Nitrite prediction by O-PLS model using optimal wavelengths

Based on the selected optimal wavelengths, the F-PLS model using full raw spectra was optimized, and the RC-O-PLS model with 19 optimal wavelengths selected by RC and the SPA-O-PLS model with 15 optimal wavelengths selected by SPA were respectively established. The specific performances of the two optimized models are shown in Table 3.

In the RC-O-PLS model, the matrix with 104×9 (samples×wavelengths) was used for calibration, and the matrix with the rest 52 samples×19 wavelengths was used for prediction. The RC-O-PLS model had a good performance with the r_C, r_{CV}, r_P of 0.92, 0.88, 0.89 and the RMSEC, RMSECV, RMSEP of 0.42 mg/kg, 0.50 mg/kg and 0.49 mg/kg, respectively. Although the wavelength numbers reduced from 486 to 19, the ability of RC-O-PLS model in predicting nitrite contents in ham sausages was similar to the F-PLS models with full wavelength. However, ΔE value in the RC-O-PLS model slightly increased and the RPD value slightly reduced compared with the original PLSR model, which may be the wavelength number reduction. With the 19 optimal wavelengths, the RC-O-PLS model can be expressed as a linear equation below.

$$Y_{\text{RC-O-PLS}} = 4.25 - 0.30X_{902.2\text{ nm}} - 44.62X_{908.8\text{ nm}} - 5.60X_{912.1\text{ nm}} - 0.74X_{913.7\text{ nm}} + 103.95X_{918.7\text{ nm}} - 19.47X_{933.5\text{ nm}} - 145.72X_{936.8\text{ nm}} + 233.20X_{991.1\text{ nm}} + 190.66X_{1216.4\text{ nm}} - 290.17X_{1249.3\text{ nm}} - 134.61X_{1382.7\text{ nm}} - 137.69X_{1384.3\text{ nm}} - 46.38X_{1499.8\text{ nm}} + 142.32X_{1643.6\text{ nm}} + 61.68X_{1675.1\text{ nm}} - 9.37X_{1693.3\text{ nm}} - 14.07X_{1695.0\text{ nm}} + 28.87X_{1696.6\text{ nm}} + 31.42X_{1698.3\text{ nm}} \tag{2}$$

In the SPA-O-PLS model, the new matrix with the size of 104×15 (samples×wavelengths) for calibration set and 52×15 (samples×wavelengths) for prediction set. As shown in Table 3, based on the 15 optimal wavelengths, the performance of the SPA-O-PLS model is comparable to the original F-PLS model in predicting nitrite values. The *r* and RMSE values of calibration, cross-validation and prediction were similar to those of F-PLS model. According to the regression coefficients of the 15 optimal wavelengths, the SPA-O-PLS model can be expressed as a linear formula below:

$$Y_{\text{SPA-O-PLS}} = -0.67 + 14.18X_{900.5\text{ nm}} + 21.26X_{907.1\text{ nm}} - 25.20X_{908.8\text{ nm}} - 49.22X_{912.1\text{ nm}} - 35.81X_{915.4\text{ nm}} + 95.92X_{920.3\text{ nm}} - 27.96X_{922.0\text{ nm}} - 225.24X_{941.7\text{ nm}} + 261.47X_{979.6\text{ nm}} + 64.07X_{1083.2\text{ nm}} + 79.79X_{1213.2\text{ nm}} - 372.98X_{1353.0\text{ nm}} - 86.12X_{1460.2\text{ nm}} + 87.56X_{1595.6\text{ nm}} + 125.74X_{1699.9\text{ nm}} \tag{3}$$

Comparing the RC-O-PLS model and the SPA-O-PLS model, it was observed that the ability of the two models in predicting nitrite content of ham sausages was similar. But the optimal wavelength numbers of the SPA-O-PLS model were less than that of the RC-O-PLS model (15 vs. 19). Hence, from the whole results, it was suggested that the SPA-O-PLS model was more efficient and suitable for nitrite content prediction in ham sausages.

Table 3 RC-O-PLS model and SPA-O-PLS model for predicting nitrite in ham sausages using optimal wavelengths

Model	Method for wavelength selection	Number of optimal wavelength	LVs	Calibration		Cross-validation		Prediction			ΔE
				r_C	RMSEC/mg·kg^{-1}	r_{CV}	RMSECV/mg·kg^{-1}	r_P	RMSEP/mg·kg^{-1}	RPD	
RC-O-PLS	RC	19	11	0.92	0.42	0.88	0.50	0.89	0.49	2.15	0.07
SPA-O-PLS	SPA	15	10	0.92	0.41	0.89	0.49	0.89	0.49	2.15	0.08

3.6 Nitrite prediction by MLR model using optimal wavelengths

Besides PLS, multivariate linear regression (MLR) can also be used for model establishment when the number of wavelengths is less than that of samples. In this study, the MLR models based on the optimal wavelengths selected by RC (RC-MLR model) and SPA (SPA-MLR model) were respectively built and their performance of predicting nitrite content in ham sausages are shown in Table 4. The two MLR models showed good abilities for nitrite prediction and the accuracy similar.

Compared with the RC-O-PLS model and SPA-O-PLS model, the two MLR models also had similar results for calibration, cross-validation and prediction. In terms of acceleration of the speed of data calculation and model establishment, the SPA-MLR model would be better among the simplified models for nitrite prediction in ham sausages. The *F*-test on the result of SPA-MLR was conducted for the sake of statistical soundness. As shown in Table 5, the *F*-value is 1.13>1 which indicates the test on the right side, *F*<"*F* (one-tailed critical value)=1.60, *p* (*F*≤*f*)=0.33>0.05, and there is no significant difference in precision between the two groups of data (reference value and predicted value). SPA-MLR model can be expressed as a linear formula below:

$$Y_{\text{SPA-MLR}} = -0.52 + 17.81X_{900.5\text{ nm}} + 25.80X_{907.1\text{ nm}} - 49.60X_{908.8\text{ nm}} - 40.71X_{912.1\text{ nm}} - 32.88X_{915.4\text{ nm}} + 99.08X_{920.3\text{ nm}} - 19.53X_{922.0\text{ nm}} - 223.75X_{941.7\text{ nm}} + 276.84X_{979.6\text{ nm}} + 44.88X_{1083.2\text{ nm}} + 88.11X_{1213.2\text{ nm}} - 401.39X_{1353.0\text{ nm}} - 96.73X_{1460.2\text{ nm}} + 136.63X_{1595.6\text{ nm}} + 110.76X_{1699.9\text{ nm}} \tag{4}$$

Table 4 RC-MLR model and SPA-MLR model for predicting nitrite in ham sausages using optimal wavelengths

Model	Method for wavelength selection	Number of optimal wavelength	Calibration		Cross-validation		Prediction			ΔE
			r_C	RMSEC/mg·kg^{-1}	r_{CV}	RMSECV/mg·kg^{-1}	r_P	RMSEP/mg·kg^{-1}	RPD	
RC-MLR	RC	19	0.92	0.41	0.79	0.65	0.88	0.49	2.17	0.08
SPA-MLR	SPA	15	0.92	0.40	0.89	0.48	0.90	0.47	2.25	0.07

Table 5 *F*-test two-sample analysis of variance

	Reference value	Predicted value
Average	3.45	3.38
Variance	1.07	0.94
Observed value	51	51
df	50	50
F	1.13	
p(*F*≤*f*)	0.33	
"*F*(one-tailed critical value)	1.60	

Note: d*f*: degree of freedom.

4 Conclusions

In this study, the hyperspectral data in the wavelength range of 900-1700 nm for evaluating nitrite content in ham sausages was investigated. The spectral information within the ROIs of the hyperspectral images of ham sausages was extracted and averaged to relate to the measured nitrite content using PLS algorithm. After spectral pretreatment with MAS, SGS, MFS, GFS and Normalize methods, the PLS models showed good performance in the prediction of nitrite content, with high R and low RMSE. To accelerate the data analysis, 15 optimal wavelengths including 900.5 nm, 907.1 nm, 908.8 nm, 912.1 nm, 915.4 nm, 920.3 nm, 922.0 nm, 941.7 nm, 979.6 nm, 1083.2 nm, 1213.2 nm, 1353.0 nm, 1460.2 nm, 1595.6 nm and 1699.9 nm were selected from the raw spectra by SPA to simplify the original PLS model, and the SPA-MLR model based on the 15 wavelengths were finally built and showed better performance in predicting nitrite content of ham sausages (r_P=0.90, RMSEP=0.47 mg/kg, RPD=2.25). The whole results indicated that hyperspectral data in the range of 900-1700 nm can be mined for nitrite assessment in ham sausages, which will provide data support for the development of multispectral imaging inspection in the future online and offline application. In practice, when the same model is used in different devices, compatibility should be considered.

Acknowledgements

The authors acknowledge that this work was financially supported by the Key Scientific and Technological Project of Henan Province (Grant No. 212102310491; No. 182102310060), Major Scientific and Technological Project of Henan Province (No. 161100110600), China Postdoctoral Science Foundation (No. 2018M632767), Henan Postdoctoral Science Foundation (No. 001801021), Youth Talents Lifting Project of Henan Province (No. 2018HYTP008).

[References]

[1] Talens P, Mora L, Morsy N, Barbin D F, ElMasry G, Sun D W. Prediction of water and protein contents and quality classification of Spanish cooked ham using NIR hyperspectral imaging. Journal of Food Engineering, 2013; 117(3): 272–280.

[2] Gong A P, Zhu S S, He Y, Zhang C. Grading of Chinese Cantonese sausage using hyperspectral imaging combined with chemometric methods. Sensors, 2017; 17(8): 1706.

[3] Majou D, Christieans S. Mechanisms of the bactericidal effects of nitrate and nitrite in cured meats. Meat Science, 2018; 145: 273–284.

[4] Sudarvizhi A, Pandian K, Oluwafemi O S, Gopinath S C B. Amperometry detection of nitrite in food samples using tetrasulfonated copper phthalocyanine modified glassy carbon electrode. Sensors & Actuators B: Chemical, 2018; 272: 151–159.

[5] Sudarvizhi A, Siddiqha Z A, Pandian K. Single step synthesis of graphene oxide protected silver nanoparticles using aniline as reducing agent and study its application on electrocatalytic detection of nitrite in food samples. J Chem Applied Biochem, 2014; 1: 101.

[6] Kim H S, Hur S J. Changes in the mutagenicity of heterocyclic amines, nitrite, and N-nitroso compound in pork patties during in vitro human digestion. LWT, 2018; 92: 47–53.

[7] Moorcroft M J, Davis J, Compton R G. Detection and determination of nitrate and nitrite: a review. Talanta, 2001; 54(5): 785–803.

[8] Feng C H, Makino Y, Yoshimura M, Thuyet D Q. Hyperspectral imaging in tandem with R statistics and image processing for detection and visualization of pH in Japanese big sausages under different storage conditions. Journal of Food Science, 2018; 83(2): 358–366.

[9] Jiang H, Wang W, Ni X, Zhuang H, Yoon S C, Lawrence K C. Recent advancement in near infrared spectroscopy and hyperspectral imaging techniques for quality and safety assessment of agricultural and food products in the China Agricultural University. NIR news, 2018; 29(8): 19–23.

[10] He H, Wu D, Sun D. Rapid and non-destructive determination of drip loss and pH distribution in farmed Atlantic salmon (*Salmo salar*) fillets using visible and near-infrared (Vis-NIR) hyperspectral imaging. Food Chemistry, 2014; 156: 394–401.

[11] Feng C H, Makino Y, Oshita S, Martín J F G. Hyperspectral imaging and multispectral imaging as the novel techniques for detecting defects in raw and processed meat products: Current state-of-the-art research advances. Food Control, 2018; 84: 165–176.

[12] He H, Sun D. Toward enhancement in prediction of Pseudomonas counts distribution in salmon fillets using NIR hyperspectral imaging. LWT-Food Science and Technology, 2015; 62(1): 11–18.

[13] Khoshnoudi-Nia S, Moosavi-Nasab M, Nassiri S M, Azimifar Z. Determination of total viable count in rainbow-trout fish fillets based on hyperspectral imaging system and different variable selection and extraction of reference data methods. Food Analytical Methods, 2018; 11(12): 3481–3494.

[14] Kamruzzaman M, Makino Y, Oshita S. Online monitoring of red meat color using hyperspectral imaging. Meat Science, 2016; 116: 110–117.

[15] Achata E M, Inguglia E S, Esquerre C A, Tiwari B K, O'Donnell C P. Evaluation of Vis-NIR hyperspectral imaging as a process analytical tool to classify brined pork samples and predict brining salt concentration. Journal of Food Engineering, 2019; 246: 134–140.

[16] Cheng W W, Sun D W, Pu H B, Wei Q Y. Interpretation and rapid detection of secondary structure modification of actomyosin during frozen storage by near-infrared hyperspectral imaging. Journal of Food Engineering, 2019; 246: 200–208.

[17] Feng C H, Makino Y, Yoshimura M, Rodríguez-Pulido F J. Estimation of adenosine triphosphate content in ready-to-eat sausages with different storage days, using hyperspectral imaging coupled with R statistics. Food Chemistry, 2018; 264: 419. doi: 10.1016/j.foodchem.2018.05.029.

[18] Stachniuk A, Szmagara A, Stefaniak E A. Spectrophotometric assessment of the differences between total nitrate/nitrite contents in peel and flesh of cucumbers. Food Analytical Methods, 2018; 11(10): 2969–2977.

[19] Liu Y W, Sun D W, Cheng J H, Han Z. Hyperspectral imaging sensing of changes in moisture content and color of beef during microwave heating process. Food Analytical Methods, 2018; 11(9): 2472–2484.

[20] He J, Chen L, Chu B, Zhang C. Determination of total polysaccharides and total flavonoids in *Chrysanthemum morifolium* using near-infrared hyperspectral imaging and multivariate analysis. Molecules, 2018; 23(9): 2395. doi: 10.3390/molecules23092395.

[21] Giacomo D R, Stefania D Z. A multivariate regression model for detection of fumonisins content in maize from near infrared spectra. Food Chemistry, 2013; 141(4): 4289–4294.

[22] He H, Wu D, Sun D. Non-destructive and rapid analysis of moisture distribution in farmed Atlantic salmon (*Salmo salar*) fillets using visible and near-infrared hyperspectral imaging. Innovative Food Science & Emerging Technologies, 2013; 18: 237–245.

[23] Siripatrawan U. Hyperspectral imaging for rapid evaluation and visualization of quality deterioration index of vacuum packaged dry-cured sausages. Sensors and Actuators B: Chemical, 2018; 254: 1025–1032.

[24] Cheng J, Sun D. Rapid quantification analysis and visualization of *Escherichia coli* loads in grass carp fish flesh by hyperspectral imaging method. Food and Bioprocess Technology, 2015; 8(5): 951–959.

[25] Jiang S Q, He H J, Ma H J, Chen F S, Xu B C, Liu H, et al. Quick assessment of chicken spoilage based on hyperspectral NIR spectra combined with partial least squares regression. Int J Agric & Biol Eng, 2021; 14(1): 243–250.

[26] He H, Sun D, Wu D. Rapid and real-time prediction of lactic acid bacteria (LAB) in farmed salmon flesh using near-infrared (NIR) hyperspectral imaging combined with chemometric analysis. Food Research International, 2014; 62: 476–483.

[27] He H, Sun D. Selection of informative spectral wavelength for evaluating and visualising Enterobacteriaceae contamination of salmon flesh. Food Analytical Methods, 2015; 8(10): 2427–2436.

[28] Araújo M C U, Saldanha T C B, Galvão R K H, Yoneyama T, Chame H C, Visani V. The successive projections algorithm for variable selection in spectroscopic multicomponent analysis. Chemometrics and Intelligent Laboratory Systems, 2001; 57(2): 65–73.

[29] Wu D, Shi H, Wang S, He Y, Bao Y D, Liu K S. Rapid prediction of moisture content of dehydrated prawns using online hyperspectral imaging system. Analytica Chimica Acta, 2012; 726: 57–66.

[30] Cozzolino D, Murray I. A review on the application of infrared technologies to determine and monitor composition and other quality characteristics in raw fish, fish products, and seafood. Applied Spectroscopy Reviews, 2012; 47(3): 207–218.

[31] Wu D, Wang S J, Wang N F, Nie P C, He Y, Sun D W, et al. Application of time series hyperspectral imaging (TS-HSI) for determining water distribution within beef and spectral kinetic analysis during dehydration. Food and Bioprocess Technology, 2013; 6(11): 2943–2958.

[32] Fernández-Cabanás V M, Polvillo O, Rodríguez-Acuña R, Botella B, Horcada A. Rapid determination of the fatty acid profile in pork dry-cured sausages by NIR spectroscopy. Food Chemistry, 2011; 124(1): 373–378.

[33] Nicolaï B M, Beullens K, Bobelyn E, Peirs A, Saeys W, Theron K I, et al. Nondestructive measurement of fruit and vegetable quality by means of NIR spectroscopy: A review. Postharvest Biology and Technology, 2007; 46(2): 99–118.

[34] Feng Y, Sun D. Near-infrared hyperspectral imaging in tandem with partial least squares regression and genetic algorithm for non-destructive determination and visualization of Pseudomonas loads in chicken fillets. Talanta, 2013; 109: 74–83.

[35] Feng C, Makino Y, Yoshimura M, Rodriguez-Pulido F J. Real-time prediction of pre-cooked Japanese sausage color with different storage days using hyperspectral imaging. Journal of the Science of Food and Agriculture, 2018; 98(7): 2564–2572.